HHS Public Access

Author manuscript

Cancer Res. Author manuscript; available in PMC 2017 January 15.

Published in final edited form as:

Cancer Res. 2016 January 15; 76(2): 377–389. doi:10.1158/0008-5472.CAN-14-2814.

Characterization of a c-Rel inhibitor that mediates anticancer properties in hematologic malignancies by blocking NF-κB-controlled oxidative stress responses

Yusuke Shono[1], **Andrea Z. Tuckett**[1], **Hsiou-Chi Liou**[2,3], **Ekaterina Doubrovina**[4], **Enrico Derenzini**[5], **Samedy Ouk**[2], **Jennifer J. Tsai**[1], **Odette M. Smith**[1], **Emily R. Levy**[1], **Fabiana M. Kreines**[1], **Carly G.K. Ziegler**[1,6], **Mary I. Scallion**[5], **Mikhail Doubrovin**[4], **Glenn Heller**[7], **Anas Younes**[5], **Richard J. O'Reilly**[4], **Marcel R.M. van den Brink**[1,5,8], and **Johannes L. Zakrzewski**[4,8]

[1]Department of Immunology, Memorial Sloan Kettering Cancer Center, San Diego, CA

[2]ImmuneTarget Inc., San Diego, CA

[3]ImmuneTarget Inc., New York, NY

[4]Department of Pediatrics, Memorial Sloan Kettering Cancer Center, New York, NY

[5]Department of Medicine, Memorial Sloan Kettering Cancer Center, New York, NY

[6]Department of Computational Biology, Memorial Sloan Kettering Cancer Center, New York, NY

[7]Department of Epidemiology and Biostatistics, Memorial Sloan Kettering Cancer Center, New York, NY

Abstract

NF-κB plays a variety of roles in oncogenesis and immunity that may be beneficial for therapeutic targeting, but strategies to selectively inhibit NF-κB to exert antitumor activity have been elusive. Here we describe IT-901, a bioactive naphthalenethiobarbiturate derivative that potently inhibits the NF-κB subunit c-Rel. IT-901 suppressed graft-versus-host disease while preserving graft-versus-lymphoma activity during allogeneic transplantation. Further preclinical assessment of IT-901 for the treatment of human B cell lymphoma revealed antitumor properties in vitro and in vivo without restriction to NF-κB-dependent lymphoma. This non-discriminatory, anti-lymphoma effect was attributed to modulation of the redox homeostasis in lymphoma cells resulting in oxidative stress. Moreover, NF-κB inhibition by IT-901 resulted in reduced stimulation of the oxidative stress response gene heme oxygenase-1, and we demonstrated that NF-κB inhibition exacerbated oxidative stress induction to inhibit growth of lymphoma cells. Notably, IT-901 did

Correspondence should be addressed to: Johannes L Zakrzewski (JLZ), ZakrzewJ@mskcc.org, Office: 212-639-3267, Fax: 212-717-3447, Memorial Sloan Kettering Cancer Center, 1275 York Avenue, New York, NY 1006.

[8]These authors contributed equally to this work.

Conflict of Interest:

H.L. is a co-founder of ImmuneTarget Inc. and S.O. is the C.E.O of ImmuneTarget, Inc. J.L.Z. is a consultant/advisory board member of ImmuneTarget, Inc. No potential conflicts of interest were disclosed by the other authors.

Disclosure of Potential Conflicts of Interest

H.L. is a co-founder of ImmuneTarget, Inc. J.L.Z. is a consultant/advisory board member of ImmuneTarget, Inc. No potential conflicts of interest were disclosed by the other authors.

not elicit increased levels of reactive oxygen species in normal leukocytes, illustrating its cancer selective properties. Taken together, our results provide mechanistic insight and preclinical proof of concept for IT-901 as a novel therapeutic agent to treat human lymphoid tumors and ameliorate graft-versus-host disease.

Introduction

Amongst its many functions, nuclear factor (NF)-κB plays important roles in immunity (1–6) and oncogenesis (1, 7), indicating that therapeutic targeting of this pathway could be beneficial in a variety of clinical settings; however, an NF-κB-specific inhibitor does not exist in clinical practice to date. One approach toward development of such a compound is small-molecule-mediated direct inhibition of one or several members of the NF-κB family of transcription factors, a network that comprises five structurally related proteins including p50 (NF-κB1), p52 (NF-κB2), p65 (RelA), RelB and c-Rel (8).

After screening of a library of 15,000 small molecules with a biochemical assay measuring inhibition of c-Rel interaction with its high-affinity DNA binding site, we identified two scaffolds with inhibitory activity for the NF-κB family of transcription factors and particularly high specificity for the transcription factor c-Rel. These scaffolds, thiohydantoin and napthalenethiobarbitutate, act as direct NF-κB inhibitors by preventing DNA binding of the c-Rel protein. We previously reported that *in vitro* treatment of T cells with the thiohydantoin IT-603 induces c-Rel deficiency, resulting in suppression of T cell alloactivation without compromising T cell activation triggered by recognition of tumor-associated or viral antigens (9). Here, we demonstrate significant *in vivo* efficacy of the naphthalenethiobarbiturate IT-901 in mouse models of graft-versus-host disease (GVHD) and graft-versus-lymphoma (GVL), as well as a xenograft model of human B cell lymphoma, revealing that IT-901 treatment results not only in suppression of GVHD while retaining GVL activity, but it also mediates promising anti-lymphoma effects. We characterize pharmacokinetic (PK) and toxicology profiles as well as the mechanism of action of IT-901 mediated anti-lymphoma activity in human diffuse large B cell lymphoma (DLBCL) cells, thereby laying the groundwork for the development of a new drug combining unique immunomodulatory and antineoplastic properties.

Materials and Methods

Mice and bone marrow transplantation

We obtained female C57BL/6 (B6, H-2^b), BALB/c (H-2^d) from the Jackson Laboratory. Male *NOD/scid/IL2Rγ*(null) (NSG) mice were purchased from the Jackson Laboratory. BALB/C-Tg(NFkB-RE-luc)-Xen mice were obtained from Taconic. B6 mice carrying the *c-Rel* gene null mutation (*c-Rel*$^{-/-}$) were originally generated by inserting the neomycin cassette into the fifth exon of the c-Rel gene (3). *c-Rel*$^{-/-}$ B6 mice were maintained at Memorial Sloan Kettering Cancer Center in accordance with Institutional Animal Care and Use Committee Standards. Mice used for experiments were 6–9 weeks old. Mouse HSCT experiments were performed as previously described (10), with 850 cGy split-dosed lethal irradiation of BALB/c recipients transplanted with bone marrow (5×10^6), T cell depleted

(TCD) with anti-Thy-1.2 and low-TOX-M rabbit complement (Cedarlane Laboratories). Mouse T cells were prepared by harvesting donor splenocytes and enriching T cells by Miltenyi MACS purification of CD5 (routinely >90% purity). In A20 lymphoma experiments, animals received tumor cells intravenously in a separate injection on day 0.

Small molecule c-Rel inhibitor compounds

Our team previously identified thiohydantoin and naphthalenethiobarbiturate derivatives as conformation-disrupting direct c-Rel inhibitors (9, 11, 12). c-Rel inhibitory activity of these small molecule compounds was confirmed by fluorescence polarization (FP) as well as electrophoretic mobility shift assay (EMSA) utilizing the DNA-binding property of the c-Rel protein. NF-κB DNA binding ELISA (*TransAM® NFκB Family* kit from Active Motif North America, see manufacturer's protocol for more details) was also used to evaluate the activation of c-Rel. To obtain an estimate of the IC_{50}, a constant amount of 32p-labeled-κB probe (1 nM, CD28RE) and c-Rel protein (5 nM) were incubated with serial dilutions of IT-901 (50 μM to 100 nM) for 20 minutes in a 20 μl reaction at room temperature. The reactions were then resolved on native polyacrylamide gel following the standard protocol described previously (13). The c-Rel inhibitors IT-603 and IT-901 were provided by ImmuneTarget Inc.

Assessment of GVHD and GVT; *in vivo* BLI

Mice were monitored daily for survival and weekly for GVHD clinical scores (14). In GVT experiments, we determined the bioluminescent signal intensity (BLI) of tumor bearing mice twice weekly as described previously (15). We superimposed pseudocolor images showing the whole-body distribution of bioluminescent signal intensity on grayscale photographs and determined total flux (photons s^{-1}) for individual mice. We determined the cause of death (tumor versus GVHD) by necropsy and histopathology as previously described (16).

Cell lines and primary cells

A20, a B cell lymphoma cell line of BALB/c origin was kindly provided by A. Houghton (Memorial Sloan Kettering Cancer Center). We retrovirally transduced A20 to express a triple fusion protein consisting of herpes simplex virus thymidine kinase, enhanced green fluorescent protein and firefly luciferase (TGL) as described previously (17). The human DLBCL-derived cell lines SU-DHL4, OCI-Ly19, U2932 were obtained from the German Collection of Microorganisms and Cell Cultures, Department of Human and Animal Cell Cultures (Braunschweig, Germany); SU-DHL8 cells, were obtained from ATCC. The HBL1 and TMD8 cells were kindly provided by Dr. R.E. Davis (Houston, Tx), and authenticated before using them by the MD Anderson Characterized Cell Lines Core Facility. Cell lines were cultured in RPMI 1640 medium supplemented with 10 to 20% heat-inactivated fetal bovine serum (GIBCO BRL, Gaithersburg, MD), 1% L-glutamine, and penicillin-streptomycin in a humid environment of 5% CO_2 at 37°C. An NF-κB/Jurkat/GFP transcriptional reporter cell line (18) was purchased from System Biosciences (Mountain View, CA). Cells were stimulated with human TNF-alpha (10ng/ml) and incubated in the presence of IT-603, IT-901, or empty vehicle for 20 hours. NF-κB activity (GFP fluorescence intensity) and viability (based on DAPI) were analyzed by flow cytometry.

Combined data from three independent experiments are presented. Human $CD19^+$ peripheral blood mononuclear cells (PBMC) were purchased from United States Biological (Salem, MA). Human primary B cell lymphoma and T cell lymphoma cells were obtained from the Hematology/Oncology Tissue Bank at Memorial Sloan Kettering Cancer Center. Sample and patient data collection were approved by the Human Biospecimen Utilization Committee and the Institutional Review Board/Privacy Board-B of Memorial Sloan Kettering Cancer Center.

Human EBV-transformed B lymphoblastoid cells were generated from PBMC of a healthy donor. Human EBV-specific T cells were generated from PBMC of the same donor by repeated *in vitro* stimulations with an autologous EBV-transformed B cells.

Serum cytokines analyses

Blood was collected into microcentrifuge tubes, allowed to clot and centrifuged, and the supernatant was collected. Multiplex ELISA was conducted per manufacturer's instructions (Millipore). Results were acquired with a Luminex 200 instrument and analyzed with xPONENT software (Luminex Corporation).

Antibodies and flow cytometry

All antibodies other than the anti-c-Rel, anti-p50, anti-p52 antibodies (Santa Cruz Biotechnology), and the anti-CD44, anti-p65 antibodies (Biolegend) were obtained from BD Biosciences – Pharmingen. For cell analysis of surface markers, cells were stained for 20 minutes at 4° in PBS with 0.5% BSA (PBS/BSA) after Fc block, washed, and resuspended in DAPI in PBS/BSA. Cell surface staining was followed by intracellular staining with the eBioscience kit per manufacturer's instructions. Dead cells were excluded with LIVE/DEAD Fixable Dead Cell Stain kit (Invitrogen). Intranuclear c-Rel staining was performed as previously described (9). All flow cytometry was performed on an LSR II (BD Biosciences) and analyzed with FlowJo (TreeStar Software). Human anti-adalimumab was purchased from AbD Serotec (Bio-Rad Laboratories, Inc).

MTS assay

Relative cell growth was measured by *CellTiter 96 Aqueous Non-Radioactive Cell Proliferation Assay* (Promega) per manufacturer's instructions. Briefly, tetrazolium compound [3-(4,5-dimethylthiazol-2-yl)-5-(3-carboxymethoxyphenyl)-2-(4-sulfophenyl)-2H-tetrazolium, inner salt; MTS] was added to the culture media and the conversion of MTS into formazon was measured by the amount of 490nm absorbance. The number of viable cells correlates with absorbance at 490nm (see manufacturer's protocol for more details).

Quantitative PCR

Reverse transcription-PCR was performed with iScript Advanced cDNA Synthesis Kit for RT-qPCR (BIO-RAD). For real-time PCR, NF-κB signaling pathway Plus PrimePCR Pathway Plate was used per manufacturer's instructions (BIO-RAD). PCR was done on CFX96 Touch Real-Time PCR (BIO-RAD) with Universal SYBR Green Supermix (BIO-

RAD). Relative amount of HMOX1 was calculated by the comparative ΔC(t) method utilizing CFX Manager Software (BIO-RAD).

Heme oxygenase-1 (HMOX1) enzyme-linked immunosorbent assay

In order to measure HMOX1 protein level in IT-901 treated Ly19 human DLBCL, Ly19 cells were lysed with extraction reagent included in the *HO-1 Human ELISA Kit* (abcam). Analysis was performed per manufacturer's instructions. Optical density (OD) was determined, using a microplate autoreader (Bio-Tek Optiplex 755 Microplate Reader) at 450 nm. HMOX1 protein concentration of the samples was determined based on a specific HMOX1 standard curve.

Mouse IL-2 enzyme-linked immunosorbent assay

IL-2 production by activated T cells was measured with the *Mouse IL-2 ELISA Kit* purchased from Sigma-Aldrich (St. Louis, MO). Wild-type C57BL/6 mouse splenocytes were treated with different concentrations of IT-901 or empty vehicle for one hour and stimulated *in vitro* with anti-CD3/CD28 for 5 hours. Cell culture supernatants were analyzed for IL-2 per the manufacturer's instructions.

Inducible nitric oxide synthase (iNOS) enzyme-linked immunosorbent assay

An ELISA-based assay was performed to measure total iNOS in IT-901 treated human DLBCL including Ly19, SU-DHL8, and TMD8 cells. Cells were treated *in vitro* with IT-901 (4μM) or control solution for 24 hours in a 96-well microplate. After fixation of cells in the wells, iNOS levels were determined using *Human Total iNOS Cell-Based ELISA* (R&D Systems) per manufacturer's instructions.

Detection of reactive oxygen species and treatment with *N*-Acetyl-L-cysteine

B cell lymphoma cells were treated *in vitro* with IT-901 (4μM) or control solution for different time periods to induce reactive oxygen species (ROS) generation. ROS levels were analyzed by utilizing the Image-iT LIVE Green Reactive Oxygen Species Detection Kit (Molecular Probes, Invitrogen) per manufacturer's instructions. ROS levels were analyzed by quantifying a fluorogenic marker (carboxy-H_2DCFDA) using flow cytomertry (LSR II, BD Bioscience). *N*-Acetyl-L-cysteine was purchased from SIGMA-ALDRICH. For microscopic detection of ROS, IT-901 treated cells were stained with carboxy-H_2DCFDA, MitoTracker Deep Red FM (Life Technologies), and Hoechst 33342 (Life Technologies), followed by laser scanning confocal microscopy on a Leica SP5 confocal microscope.

Detection of reactive oxygen and reactive nitrogen species

Analyses of superoxide, hydrogen peroxide and reactive nitrogen levels were performed with IT-901 treated human DLBCL including Ly19, SU-DHL8, and TMD8 cells. Cells were treated *in vitro* with IT-901 (4μM) or control solution for 24 hours and the levels of superoxide, hydrogen peroxide and reactive nitrogen were determined by *MitoSOX Red Mitochondrial Superoxide Indicator*, *Premo Cellular Hydrogen Peroxide Sensor*, and *DAF-FM Diacetate*, respectively per manufacturer's instructions (Life Technologies). The

fluorescence intensities of cells after treatment were detected by flow cytomertry (LSR II, BD Bioscience).

Glutathione Assay

Ly19, SUDH8, and TMD8 cells were treated with IT-901 at 4μM or control vehicle for 24 hours and cells were analyzed for total and oxidized glutathione by *HT Glutathione Assay Kit* (Trevigen Inc.) per the manufacturer's protocol. Reduced GSH was calculated by subtracting oxidized GSSG from total glutathione.

Mitochondrial respiration assay

Real-time measurement of oxygen consumption rate (OCR) and extra-cellular acidification rate (ECAR) in Ly19 cells were conducted in a XF96 extracellular flux analyzer (Seahorse Bioscience, North Billerica, MA). Briefly, Ly19 cells treated either with IT-901 at 4μM or control vehicle 3 to 24 hours were washed with RPMI-1640 supplemented with 10% fetal bovine serum and L-glutamine, resuspended in mitochondria stress medium (DMEM supplemented with 10 mM glucose, 1 mM pyruvate, 2 mM glutamine, pH 7.35) and transferred to a XF96 cell culture microplates (Seahorse Bioscience) pre-treated with Cell-Tak (BD Biosciences) at a density of 200,000 cells per well. After incubation at 37°C in the absence of CO2 for 1hr in a Prep Station incubator Station, real-time measurements of OCR were collected at intervals of 4 minutes as a parameter of mitochondrial respiration. The standard assay was carried out and used the compounds stock provided in the *XF Cell Mito Stress Test Kit.* After optimization of oligomycin and FCCP working concentration the mitochondrial stress assay was conducted following the manufacturer's instructions.

c-Rel knockdown with shRNA

An optimized microRNA backbone (miR-E) for effective c-Rel knockdown was designed according to a previous report (19). We designed twelve different sequences for efficient c-Rel targeting by shRNA and utilized two (#2131 and #2205) in our experiments to analyze HMOX1 level in c-Rel knockeddown Ly19 lymphoma cells. 97-mir sequences of the two shRNAs are TGCTGTTGACAGTGAGCGACAGCATTTTGTATTTGTCTAATAGTGAAGCCACAG AT GTATTAGACAAATACAAAATGCTGCTGCCTACTGCCTCGGA (#2131) and TGCTGTTGACAGTGAGCGCAATACTGTATTTGAGAATATATAGTGAAGCCACAG AT GTATATATTCTCAAATACAGTATTATGCCTACTGCCTCGGA (#2205). Ly19 cells were resuspended in lentivirus-containing supernatant in the presence of polybrene (4 ng/μl) and incubated at 37°C in a CO_2 incubator for 24 hours. Transduced cell populations were selected 7 days post infection using 0.5 ng/μl puromycin (Sigma-Aldrich).

Analysis of c-Rel gene expression in human cells

c-Rel expression data from human primary cells and cell lines were ontained from several publically available databases. Microarray data normalized by RMA and RNA sequencing data normalized by RPKM were obtained from The Broad Institute of MIT and Harvard (20, 21).

Pharmacokinetics

Plasma samples were analyzed at 30 minutes, 1, 2, 4, 6, and 16 hours after intraperitoneal, subcutaneous or oral administration of 12–20 mg/kg of c-Rel inhibitor compound IT-603 and IT-901. To assess the level of IT-603 and IT-901 in blood, samples were analyzed by liquid chromatography-tandem mass spectrometry (LC-MS/MS) as previously described (22, 23). Calibration curves were determined for IT-603 to permit conversion of peak areas to the drug amounts against external reference standards. The tandem MS/MS detector (Model ABI/Sciex API 4000, Applied Biosystem, Foster City, California) permitted verification of peak identity as well as a quantitative assessment of the compounds in the samples.

Xenograft model of EBV-induced B cell lymphoma

Male NSG mice received 5×10^6 EBV-transformed B lymphoblastoid cells that were transduced to express firefly luciferase via subcutaneous injection on the back left side above the hind leg. On day 8 after tumor challenge animals were assigned to the different groups and treatment with IT-901, vehicle, and / or EBV-specific human T cells was initiated. 2,000 units of human interleukin 2 were administered i.p. to all animals three times per week starting on day 8 after tumor challenge. Tumor progression was monitored by in vivo BLI and by caliper measurement. Animals were sacrificed when tumors became ulcerated.

Statistics

Data are presented as mean ± s.e.m. Survival curves were analyzed with the Mantel-Cox log-rank test. For longitudinal *in vivo* studies measuring tumor volume, mice were randomly assigned to the treatment groups and the area under the curve (AUC) was used to summarize the trajectory of the measured value of each mouse under study. Not all the mice were followed for the full length of the study. The primary reason for censoring was death or sacrifice, and ignoring this type of informative censoring may result in a biased treatment comparison. To eliminate this bias, a test statistic was used that is formed based on the information up to the minimum follow up time for each cross treatment mouse pair. By eliminating the uneven censorship between mouse pairs in different groups, a test statistic can be constructed that has mean zero when the growth rates in the two groups are equal. The statistic is based on the average difference in the censored AUC curves between treatment groups. P-values were generated from a permutation test, using the AUC and log rank test statistics. The application of the permutation procedure was due to the “small” number of animals in these studies. For nonsurvival pointwise analyses, unpaired *t* test was used for comparisons between two experimental groups, or nonparametric Mann-Whitney U test was used for non-Gaussian distributions, and ANOVA was used for comparisons of more than two groups. A *P* value of less than 0.05 was considered statistically significant.

Results

The c-Rel inhibitor IT-901 is a promising small molecule for drug development

We previously introduced the thiohydantoin IT-603 as a small molecule c-Rel inhibitor, indicating that this intranuclear target is indeed druggable (9). After additional testing and structure activity relationship analysis we identified the naphthalenethiobarbiturate IT-901 (Fig. 1A) as a second chemical lead. Electrophoretic mobility shift assay (EMSA) and NF-κB DNA binding ELISA revealed that IT-901 efficiently inhibits DNA binding of c-Rel (Supplementary Fig. 1A and B). The estimated half maximal inhibitory concentration (IC_{50}) regarding global NF-κB activity was about six times lower for IT-901 (3μM) compared with IT-603 (18.8μM), and compared with several reference drugs NF-κB inhibition by IT-901 was only outperformed by the proteasome inhibitor bortezomib (Supplementary Fig. 2).

Both IT-603 and IT-901 are hydrophobic but can easily be dissolved in DMSO. We previously reported that IT-603/DMSO was much less toxic than IT-901/DMSO when incubating T cells for 24 hours and we therefore initially used IT-603/DMSO treatment as our standard protocol for chemical induction of c-Rel deficiency *in vitro* (9). In order to establish protocols for systemic administration of a c-Rel inhibitor drug in preclinical models, we formulated IT-603 and IT-901 with the U.S. Food and Drug Administration (FDA)-approved nonionic surfactant Cremophor as the vehicle for PK studies. We found that intraperitoneally (i.p.) injected IT-901 had a superior PK profile compared to IT-603 (Supplementary Fig. 3). Utilizing the PEGylated synthetic lipid 1,2-dimyristoyl-rac-glycerol-3-dodecaethylene glycol (GDM-12) (24) for compound formulation we further improved the PK profile of IT-901 (Fig. 1B) by increasing the half-life ($T_{1/2}$) and peak-concentration (C_{max}) (Fig. 1C). Of note, both oral (p.o.) and especially subcutaneous (s.c.) administration of IT-901 resulted in much lower serum levels compared to i.p. administration (Fig. 1D).

We next compared the *in vitro* efficacy of IT-901/GDM12 versus IT-603/GDM-12 in a T cell-based assay (please note that the IC_{50} identified in these experiments will be different from the ones obtained by experiments utilizing DMSO as vehicle and/or biochemical instead of cell-based assays). Interleukin 2 (IL-2) is a well-known c-Rel target gene in activated T cells (2, 3, 9). We therefore used both flow cytometry and ELISA to measure IL-2 expression in activated T cells to assess the efficacy of our c-Rel inhibitor compounds dissolved in 3% GDM-12. As expected, we found that IT-901 was again more potent than IT-603 (Fig. 1E, Supplementary Fig. 3). The IC_{50} of IT-901/GDM-12 was 2.9 μM for c-Rel whereas IL-2 secretion was successfully blocked at 5 μM (Fig. 1F). Importantly, in contrast to our previous observations with DMSO as the vehicle, cell viability was not compromised following 24 hours of incubation in the presence of IT-901/GDM-12 at concentrations up to 10 μM (Fig. 1G and H). However, we noticed that concentrations above 10 μM become increasingly toxic and may lead to apoptosis of healthy cells.

In order to confirm the inhibitory effect of IT-901 on NF-κB pathway activity both *in vitro* and *in vivo*, we utilized BALB/c-Tg(NFκB-RE-luc)-Xen mice that carry a transgene containing NF-κB responsive elements and modified firefly luciferase cDNA (25). Incubation of lipopolysaccharide (LPS)-stimulated splenocytes from *NFκB-RE-luc* mice in

the presence or absence of c-Rel inhibitors demonstrated inhibition of NF-κB activity by both IT-603 and IT-901, again showing stronger inhibition by IT-901 (Fig. 1I and J). Moreover, *NFκB-RE-luc* mice injected with LPS following a single dose of IT-901 (Fig. 1K) showed significant inhibition of NF-κB activity seven hours after treatment (Fig. 1L), confirming that IT-901 inhibits c-Rel/NF-κB both *in vitro* and *in vivo*.

c-Rel inhibitor administration is an effective treatment of acute GVHD without impairing anti-tumor activity

Next, we performed toxicology studies demonstrating that healthy C57BL/6 mice treated with i.p. or high-dose p.o. (150 mg/kg) IT-901 for 14 days had no clinical symptoms and no changes in their numbers of splenocytes, thymocytes, and T cell subsets (Supplementary Fig. 5 and Supplementary Table 1). However, when administering IT-901 daily i.p. for more than two weeks we observed diarrhea, ruffled fur, and up to 10% weight loss.

Based on previous work by us and others (9, 26) we hypothesized that systemically administered IT-901 may be efficacious in the treatment of acute GVHD, an immunological disorder that critically depends on NF-κB and specifically c-Rel activity for T cell activation by alloantigens (9). We chose a treatment dose of 24 mg/kg based on our PK studies and dose-response *in vitro* data, with the goal of reaching IT-901 serum levels within the expected therapeutic range (0.5–1 μg/ml, equivalent to 1.5–3 μM). Initiation of i.p. IT-901 treatment within one week after HSCT was poorly tolerated and therefore not feasible. This phenomenon can likely be attributed to the low level of stress tolerance of mice in the immediate time period post lethal irradiation. Moreover, NF-κB inhibition in the setting of acute exposure to high-dose irradiation may sensitize tissues such as the intestinal epithelium to radiotoxicity (27). When initiating treatment after day seven post HSCT, gut toxicity was still dose limiting, precluding daily inhibitor administrations (not shown). However, administration every other day starting on day eight after HSCT was well tolerated and effectively improved the severity of lethal acute GVHD (Fig. 2A and Supplementary Fig. 6). Of note, IT-901 was again more efficacious than IT-603, and the therapeutic benefit was sustained even after cessation of c-Rel inhibitor treatment. Moreover, IT-901 treatment did not abolish the antitumor activity of donor T cells (Fig. 2B and C), reinforcing our previous observation that inhibition of c-Rel activity improves GVHD without impairing anti-tumor responses (9). Consistent with our previous results with IT-603, we demonstrated an increase of the percentage of donor regulatory T cells following IT-901 treatment during GVHD, but otherwise no differential effect on the immune status of the recipients (Fig. 2D and Supplementary Fig. 7).

IT-901 inhibits tumor growth in a xenograft model of human EBV-induced B cell lymphoma

Rel/NF-κB proteins can act as oncogenic transcription factors by contributing to tumor growth, survival, drug resistance, and metastasis (1, 7). The combination of c-Rel inhibition and T cell therapy may therefore not only be advantageous in that this immunomodulatory approach allows for the separation of GVHD from GVL activity, but inhibition of c-Rel activity may also display a direct antineoplastic effect. Recent genetic evidence has established a role for NF-κB signaling in lymphoid malignancies (28). To provide a rationale for clinical application of our c-Rel inhibitor technology to lymphoid malignancies,

we analyzed c-Rel gene expression in various human cancer cells. We found particularly high expression of the c-Rel gene in human EBV-transformed B cells and diffuse large B cell lymphoma (DLBCL) cell lines (Supplementary Fig. 8A and B). Moreover, we demonstrated nuclear translocation of c-Rel (indicating constitutive c-Rel activity) in a wide range of human primary lymphoma cells, especially in DLBCL and EBV-transformed B cells (Supplementary Fig. 8C). Treatment of a human EBV-B cell lymphoblastoid cell line (BLCL) with IT-901 *in vitro* induced inhibition of cell growth, whereas the numbers of normal B lymphocytes were not altered by IT-901 treatment (Fig. 3A). We next analyzed the *in vivo* efficacy of IT-901 in a human EBV-induced B cell lymphoma xenograft model and found that treatment with IT-901 significantly inhibited tumor growth (Fig. 3B). In addition, the area of necrosis was significantly larger in tumors harvested from mice receiving IT-901 (Fig. 3C). EBV-associated lymphoma is a rare but life-threatening complication occurring mostly in severely immunocompromised patients in the setting of allogeneic HSCT (29). Immunotherapy with EBV-specific cytotoxic T lymphocytes has been shown to be an effective treatment option for this disease (30). Importantly, IT-901 treatment did not compromise the efficacy of T cell therapy in this model (Fig. 3D and Supplementary Fig. 9), underscoring that in contrast to alloimmunity, protective anti-lymphoma immunity mediated by antigen-specific T cells is not impaired by IT-901 treatment (see ref. 9 for additional mechanistic information).

IT-901 inhibits growth of human DLBCL cells

Based on gene expression profiling, it is well known that there are two molecularly distinct forms of DLBCL: activated B-like (ABC) and germinal center B-like (GCB) DLBCL (31). We therefore analyzed nuclear translocation of c-Rel as well as of three additional NF-κB family members (p50, p52, and p65) in six representative DLBCL cell lines including ABC (HBL1, TMD8, U2932) and GCB (Ly19, SU-DHL4, SU-DHL8) cell lines and found that c-Rel and overall NF-κB activity was highest in ABC DLBCL cells (Supplementary Fig. 10). Importantly, IT-901 treatment strongly suppressed constitutive c-Rel activity of DLBCL cells but had a weaker effect on p50 and p52 activity and only mildly affected p65 activity (Fig. 4A). The “cross-reactivity” of IT-901 regarding Rel proteins other than c-Rel does not come as a surprise given that this family of proteins is structurally related (32). Although IT-901 treatment decreased cell viability in a dose-dependent fashion, at least 60 percent of cells were still viable after 48 hours of IT-901 treatment (4μM) in all tested cell lines except HBL1 (Fig. 4B and C).

We next investigated if IT-901 treatment affected growth of DLBCL cells *in vitro*. To our surprise we found that IT-901 inhibited cell growth of both ABC and GCB cell lines with the IC_{50} values between 3μM to 4μM (Fig. 4D and Supplementary Fig. 11). In addition, IT-901 resulted in decreased proliferation of viable ABC and GCB DLBCL cells (determined by Ki-67 expression) (Fig. 4E). This suggests that the decreased lymphoma cell numbers in response to IT-901 treatment were not just the result of cell death but also due to slower cell growth.

Inhibition of c-Rel identifies TNF-α as a possible therapeutic target in ABC DLBCL cells

NF-κB plays an important role in the initiation and promotion of cancer by fostering an inflammatory milieu in which various cytokines aid and abet malignant transformation (33). To examine if IT-901 alters cytokine production by DLBCL cells, we analyzed cytokine levels in the supernatant after *in vitro* incubation with IT-901. As anticipated, cytokine levels were hardly detectable in GCB DLBCL cells (not shown), in contrast to ABC DLBCL cells, where TMD8 showed marked production of various cytokines. IT-901 treatment resulted in decreases of most cytokine levels in TMD8 cells, with the notable exceptions of interleukin 8 (IL-8), tumor necrosis factor (TNF)-α, and TNF-β (Fig. 4F). Interestingly, TMD8 was the only DLBCL cell line that did not show inhibited growth when cultured with IT-901 at a concentration of 3μM (Fig. 4D), suggesting that in TMD8 cells cytokines such as IL-8 and TNF-α may be increased as a mechanism to overcome c-Rel inhibition by compensatory upregulation of NF-κB-dependent survival pathways. Indeed, *in vitro* treatment of TMD8 cells with a TNF-α neutralizing antibody inhibited cell growth, and this effect was enhanced when combining TNF-α blockade with IT-901 treatment (Fig. 4G), suggesting that the TNF-α pathway may be a therapeutically exploitable target in some B cell lymphomas.

IT-901 mediates anti-lymphoma activity by selective induction of oxidative stress in lymphoma cells

The non-selective inhibitory effect of IT-901 on growth of both ABC and GCB DLBCL cells led us to conclude that an NF-κB-independent mechanism contributed to the anti-lymphoma activity of IT-901. Various interactions between the oxidative stress response and NF-κB signaling have been proposed (34). Oxidative stress is an important element of anticancer therapies, although it has been implicated in tumorigenesis as well (35, 36). Heme oxygenase-1 (HMOX1) is an oxidative stress response gene (37) whose expression is regulated by NF-κB. We found that HMOX1 gene expression was highly upregulated in DLBCL cells treated with IT-901 for six hours (Fig. 5A). Furthermore, we detected significantly increased HMOX1 protein levels in Ly19 and SU-DHL8 cells treated with IT-901 for 24 hours (Fig. 5B) suggesting that HMOX1 expression was induced, which is a hallmark of oxidative stress. Oxidative stress is mediated by reactive oxygen species (ROS) that are created by a variety of cellular processes including electron leakage from mitochondrial respiratory complexes (38). We therefore next checked for the presence of ROS in cells treated with IT-901 and found that, as expected, ROS production was largely localized within mitochondria (Fig. 5C and data not shown). Interestingly, analysis of mitochondrial respiration in Ly19 cells that were incubated with IT-901 for 24 hours revealed increased mitochondrial proton leak (equivalent with non-ATP linked oxygen consumption) (Fig. 5D). It is a well-known phenomenon that there is a positive feedback loop between ROS and proton leak, reflecting cellular adaption to oxidative stress (39). Consistent with increased proton leak, ATP-linked mitochondrial respiration was decreased in IT-901-treated cells, indicating mitochondrial dysfunction (Fig. 5E).

Oxidative stress is the result of an imbalance between generation and elimination of reactive oxygen species. One of the major ROS-scavenging systems is glutathione (GSH) (40). Given that the IT-901 molecule has redox properties, we hypothesized that IT-901 may alter

the GSH homeostasis in affected cells. Indeed, we found that the levels of reduced GSH of DLBCL cells were significantly decreased following IT-901 treatment (Fig. 5F), suggesting that depletion of the reduced GSH pool by IT-901 initiates the increase in ROS levels. Replenishing the GSH pool of DLBCL cells by the addition of the antioxidant *N*-Acetyl-L-cysteine completely reversed the inhibitory effect of IT-901 on DLBCL growth, indicating that induction of oxidative stress by GSH modulation was indeed the main factor contributing to the anti-lymphoma activity of IT-901 (Fig. 5G). IT-901 induced production of high levels of ROS in both ABC and GCB DLBCL cells (Fig. 5H). Of note, normal leukocytes generated no ROS in response to treatment with IT-901 (Fig. 5H and Supplementary Table 2), suggesting that lymphoma cells are particularly sensitive to induction of oxidative stress by IT-901. Analysis of several reactive oxygen and nitrogen species revealed that superoxide and nitric oxide (NO) but not hydrogen peroxide levels were increased in lymphoma cells treated with IT-901 (Fig. 5I). Of note, superoxide and NO react spontaneously to form the highly toxic oxidant peroxynitrite, which is known to cause lipid, protein, and DNA damage and therefore cell death (34). NO can be produced by various cell types that are capable of expressing inducible NO synthase (iNOS). iNOS is an NF-κB target gene and it has been previously shown that NF-κB activation in Burkitt lymphoma cells was associated with inhibition of NO production (41). Consistent with this report we found that treatment with the NF-κB inhibitor IT-901 increases iNOS activity in B cell lymphoma cells (Fig. 5J).

Finally, we sought to investigate the impact of c-Rel inhibition on the oxidative stress response. We hypothesized that IT-901 would not only induce oxidative stress but also suppress antioxidant genes via inhibition of NF-κB target genes involved in the oxidative stress response such as HMOX1. We treated Ly19 cells with the pro-oxidant pyocyanin to generate high levels of oxidative stress, followed by analysis of HMOX1 (using HMOX1 as a surrogate marker of the NF-κB-dependent oxidative stress response) in the presence of vehicle versus NF-κB inhibitors (IT-901 or the IKK inhibitor PS-1145 (42)) (Fig. 5K, open bars), or in the presence of mock versus c-Rel-specific shRNA (Fig. 5K, gray bars). We found that c-Rel/NF-κB inhibition with PS-1145, IT-901 or shRNA indeed modulated the oxidative stress response, exemplified by reduced HMOX1 induction in the presence of pyocyanin. We therefore next investigated if NF-κB inhibition on the setting of oxidative stress had the potential to sensitize lymphoma cells to oxidative stress-mediated cell damage. We cultured Ly19 cells in the presence of oxidative stress without NF-κB inhibition (pyocyanin alone), in the presence of NF-κB inhibition in the absence of oxidative stress (PS-1145 alone), or in the presence of oxidative stress in the setting of NF-κB inhibition (pyocyanin + PS-1145, which is equivalent to the proposed dual mechanism of IT-901) (Fig. 5L). We found that NF-κB inhibition alone had no effect on Ly19 growth, induction of oxidative stress strongly inhibited lymphoma cell growth, and combining oxidative stress and NF-κB inhibition had additive anti-lymphoma effects. The proposed effects of IT-901 on oxidative stress induction and the oxidative stress response are summarized in Figure 5M.

Discussion

Although the NF-κB pathway is involved in a multitude of physiological and pathophysiological processes affecting both hematopoietic and non-hematopoietic cells, healthy cellular steady state is not associated with NF-κB activity. A truly NF-κB-specific drug would therefore not be expected to disturb normal cell function. Clinical strategies resulting in suppression of NF-κB activity include proteasome inhibitors (43), Bruton's tyronsine kinase inhibitors (44, 45), thalidomide and its analogs (46, 47), amongst others. None of these approaches is strictly NF-κB-specific, enhancing the potential of these agents for both therapeutic and adverse effects. Increasing NF-κB specificity of a given drug would be expected to improve the safety profile, possibly at the expense of reducing efficacy for some indications (such as cancer). Here we show that small molecule-mediated inhibition of the NF-κB pathway at the transcription factor level can efficiently be accomplished *in vivo* and is associated with little toxicity. Moreover, we are able to demonstrate improved *in vivo* efficacy of a multi-dose c-Rel inhibitor treatment regimen for acute lethal GVHD. The importance of this finding should not be underestimated given the issues with proteasome and IκB kinase (IKK) inhibitors in exacerbating acute GVHD (48, 49). Furthermore, our data confirm our previous findings (9) that both anti-tumor and anti-viral activity of T cells is not compromised by c-Rel inhibitor treatment, adding to the favorable safety profile.

c-Rel is well-known for its role as an oncogenic transcription factor, contributing to constitutive NF-κB activity in a wide range of cancers (7), most notably in lymphoid malignancies (50–52). We show that c-Rel is particularly over-expressed and constitutively active in DLBCL cells and EBV-transformed B lymphoblasts. As expected, *in vitro* c-Rel inhibitor treatment modulated the cytokine profile of DLBCL cells with high NF-κB activity (ABC but not GCB DLBCL cells), consistent with a previous study describing differential effects of IKK inhibitor treatment on ABC versus GCB DLBCL cells (42). In contrast to this, IT-901 had an inhibitory effect on cell growth of both of these distinct DLBCL types, suggesting that NF-κB inhibition was not the main factor affecting lymphoma cell behavior in the presence of the small molecule. We identified an additional mechanism of action of IT-901 that takes advantage of the fact that ROS production is increased in cancer cells and that modulation of the redox homeostasis has potential to be therapeutically exploited as a method to selectively cause toxicity to cancer cells while sparing healthy tissues (40). Importantly, there is a threshold range of ROS-mediated effects on cellular function. ROS levels below the critical threshold may actually be beneficial by stimulating pro-survival signaling pathways, whereas levels exceeding the threshold become harmful and result in cell death (40, 53). We found that culturing cells in the presence of IT-901 depletes their reduced GSH pool, which impairs ROS elimination and results in superoxide accumulation in B cell lymphoma cells (but not in normal leukocytes where basal superoxide generation is negligible (54)). IT-901-mediated NF-κB inhibition further exacerbated oxidative stress in lymphoma cells by inducing iNOS activity (thereby generating nitric oxide and enabling formation of peroxynitrite) while inhibiting oxidative stress response elements that are regulated by NF-κB (as illustrated by modulation of a representative oxidative stress response gene (HMOX1)). Importantly, we were able to demonstrate additive anti-lymphoma effects of combination treatment with a pro-oxidant in the presence of an NF-κB

inhibitor. IT-901 therefore represents a novel small molecule acting as a direct c-Rel/NF-κB inhibitor with additional antineoplastic activity secondary to selective induction of oxidative stress in lymphoma cells (the latter mechanism being exacerbated by NF-κB inhibition).

Interestingly, exposing lymphoma cells to IT-901 in the presence of an antioxidant reversed the anti-lymphoma effect of the small molecule even in ABC DLBCL cell lines depending on constitutive NF-κB activity for their survival. These observations reinforce the notion that for the treatment of malignant diseases, small molecule-mediated NF-κB inhibition at the transcription factor level may not be sufficient to mediate strong anti-neoplastic activity in a single-agent treatment regimen. However, consistent with NF-κB inhibition, IT-901 modulated the cytokine profile of ABC DLBCL cells, leading us to identify TNF-α as a potential therapeutic target in activated B cell lymphomas. Combination of c-Rel/NF-κB inhibition with additional cytostatic or targeted approaches has significant potential for the development of innovative minimally toxic cancer treatment protocols. Examples for rational combination strategies include NF-κB inhibition + inhibition of upstream targets such as TNF-α (Fig. 4G), tyrosine kinases, vascular endothelial growth factor, or c-Rel inhibition + checkpoint blockade such as cytotoxic T lymphocyte antigen 4 (CTLA4) inhibition (where c-Rel inhibition could mitigate adverse effects related to increased autoreactivity in the setting of reduced peripheral tolerance).

Taken together, we introduce the novel small molecule IT-901, a compound with unique properties that may benefit allogeneic transplantation as well as cancers therapy. Due to its strong c-Rel/NF-κB inhibitory potency combined with its capacity to induce high levels of oxidative stress specifically in lymphoma cells, the overall efficacy of IT-901 is far superior to our previous drug candidate IT-603. IT-901 has significant potential as antineoplastic agent for the treatment of hematologic malignancies, especially in the setting of allogeneic HSCT where c-Rel inhibition has the added benefit of ameliorating GVHD. Moreover, our findings indicate that IT-901 is not only efficacious and well tolerated but our PK and toxicology data suggest that this molecule is a promising candidate for clinical drug development. Issues that will need to be addressed before application to human subjects include additional investigational new drug (IND)-directed toxicology studies, as well as the development of an optimized clinically acceptable formulation. We expect to be able to launch a first-in-man clinical trial within the next three years.

Supplementary Material

Refer to Web version on PubMed Central for supplementary material.

Acknowledgments

Grant Support

This research was supported by National Institutes of Health award numbers R01-HL069929 (M.V.D.B.), R01-AI100288 (M.V.D.B.), R01-AI080455 (M.V.D.B.), R01-AI101406 (M.V.D.B.), and 1K08CA160659 (J.L.Z.). The content is solely the responsibility of the authors and does not necessarily represent the official views of the National Institutes of Health. Support was also received from the Radiation Effects Research Foundation (RERF-NIAID) (M.V.D.B.), Lymphoma Research Foundation Post-Doctoral Fellowship Research Grant (Y.S.), The Leukemia Research Foundation (J.L.Z.), The MSKCC Center for Molecular Imaging and Nanotechnology (CMINT) (J.L.Z.), The Society of MSKCC (J.L.Z.), the Leukemia and Lymphoma Society (contract 6465-15))

(J.L.Z.), The Experimental Therapeutics Center of Memorial Sloan Kettering Cancer Center funded by Mr. William H. Goodwin and Mrs. Alice Goodwin, The Lymphoma Foundation, Alex's Lemonade Stand, The Geoffrey Beene Cancer Research Center at Memorial Sloan Kettering Cancer Center, and the Susan and Peter Solomon Divisional Genomics Program. We appreciate the invaluable help of the Laboratory of Comparative Pathology and the Molecular Cytology Core Facility (supported by Cancer Support Grant NCI P30-CA008748) of Memorial Sloan Kettering Cancer Center. Technical services provided by the MSKCC Small-Animal Imaging Core Facility, supported in part by NIH Cancer Center Support Grant No 2 P30 CA008748-48, are also gratefully acknowledged.

References

1. Fullard N, Wilson CL, Oakley F. Roles of c-Rel signalling in inflammation and disease. The international journal of biochemistry & cell biology. 2012; 44:851–60. [PubMed: 22405852]
2. Liou HC, Hsia CY. Distinctions between c-Rel and other NF-kappaB proteins in immunity and disease. Bioessays. 2003; 25:767–80. [PubMed: 12879447]
3. Liou HC, Jin Z, Tumang J, Andjelic S, Smith KA, Liou ML. c-Rel is crucial for lymphocyte proliferation but dispensable for T cell effector function. Int Immunol. 1999; 11:361–71. [PubMed: 10221648]
4. Visekruna A, Volkov A, Steinhoff U. A key role for NF-kappaB transcription factor c-Rel in T-lymphocyte-differentiation and effector functions. Clinical & developmental immunology. 2012; 2012:239368. [PubMed: 22481964]
5. Yu Y, Wang D, Kaosaard K, Liu C, Fu J, Haarberg K, et al. c-Rel is an essential transcription factor for the development of acute graft-versus-host disease in mice. Eur J Immunol. 2013
6. Finn PW, He H, Ma C, Mueller T, Stone JR, Liou HC, et al. Molecular profiling of the role of the NF-kappaB family of transcription factors during alloimmunity. J Leukoc Biol. 2002; 72:1054–62. [PubMed: 12429729]
7. Rayet B, Gelinas C. Aberrant rel/nfkb genes and activity in human cancer. Oncogene. 1999; 18:6938–47. [PubMed: 10602468]
8. Oeckinghaus A, Ghosh S. The NF-kappaB family of transcription factors and its regulation. Cold Spring Harbor perspectives in biology. 2009; 1:a000034. [PubMed: 20066092]
9. Shono Y, Tuckett AZ, Ouk S, Liou HC, Altan-Bonnet G, Tsai JJ, et al. A Small-Molecule c-Rel Inhibitor Reduces Alloactivation of T Cells without Compromising Antitumor Activity. Cancer discovery. 2014; 4:578–91. [PubMed: 24550032]
10. Hanash AM, Dudakov JA, Hua G, O'Connor MH, Young LF, Singer NV, et al. Interleukin-22 protects intestinal stem cells from immune-mediated tissue damage and regulates sensitivity to graft versus host disease. Immunity. 2012; 37:339–50. [PubMed: 22921121]
11. Ouk S, Liou ML, Liou HC. Direct Rel/NFkB inhibitors: structural bassis for mechanism of action. Future Med Chem. 2009; 1:1683–707. [PubMed: 21425986]
12. Liou, HC. United States Patent Application Publication. 2010. Methods and compositions for targeting c-Rel.
13. Liou HC, Sha WC, Scott ML, Baltimore D. Sequential induction of NF-kappa B/Rel family proteins during B-cell terminal differentiation. Molecular and cellular biology. 1994; 14:5349–59. [PubMed: 8035813]
14. Cooke KR, Kobzik L, Martin TR, Brewer J, Delmonte J Jr, Crawford JM, et al. An experimental model of idiopathic pneumonia syndrome after bone marrow transplantation: I. The roles of minor H antigens and endotoxin. Blood. 1996; 88:3230–9. [PubMed: 8963063]
15. Zakrzewski JL, Kochman AA, Lu SX, Terwey TH, Kim TD, Hubbard VM, et al. Adoptive transfer of T-cell precursors enhances T-cell reconstitution after allogeneic hematopoietic stem cell transplantation. Nat Med. 2006; 12:1039–47. [PubMed: 16936725]
16. Petrovic A, Alpdogan O, Willis LM, Eng JM, Greenberg AS, Kappel BJ, et al. LPAM (alpha 4 beta 7 integrin) is an important homing integrin on alloreactive T cells in the development of intestinal graft-versus-host disease. Blood. 2004; 103:1542–7. [PubMed: 14563643]
17. Terwey TH, Kim TD, Kochman AA, Hubbard VM, Lu S, Zakrzewski JL, et al. CCR2 is required for CD8-induced graft-versus-host disease. Blood. 2005; 106:3322–30. [PubMed: 16037386]

18. Egan LJ, Toruner M. NF-kappaB signaling: pros and cons of altering NF-kappaB as a therapeutic approach. Annals of the New York Academy of Sciences. 2006; 1072:114–22. [PubMed: 17057194]
19. Fellmann C, Hoffmann T, Sridhar V, Hopfgartner B, Muhar M, Roth M, et al. An optimized microRNA backbone for effective single-copy RNAi. Cell reports. 2013; 5:1704–13. [PubMed: 24332856]
20. http://www.gtexportal.org
21. http://www.broadinstitute.org/ccle
22. Clarke JL, Pao W, Wu N, Miller VA, Lassman AB. High dose weekly erlotinib achieves therapeutic concentrations in CSF and is effective in leptomeningeal metastases from epidermal growth factor receptor mutant lung cancer. Journal of neuro-oncology. 2010; 99:283–6. [PubMed: 20146086]
23. Qin W, Tao H, Chen Y, Chen Z, Wu N. Sensitive, accurate and simple liquid chromatography-tandem mass spectrometric method for the quantitation of amphotericin B in human or minipig plasma. Journal of chromatographic science. 2012; 50:636–43. [PubMed: 22562820]
24. Bista RK, Bruch RF, Covington AM. Infrared spectroscopic study of thermotropic phase behavior of newly developed synthetic biopolymers. Spectrochimica acta Part A, Molecular and biomolecular spectroscopy. 2011; 81:583–9.
25. Carlsen H, Moskaug JØ, Fromm SH, Blomhoff R. In vivo imaging of NF-kappa B activity. J Immunol. 2002; 168:41–75.
26. Sun K, Wilkins DE, Anver MR, Sayers TJ, Panoskaltsis-Mortari A, Blazar BR, et al. Differential effects of proteasome inhibition by bortezomib on murine acute graft-versus-host disease (GVHD): delayed administration of bortezomib results in increased GVHD-dependent gastrointestinal toxicity. Blood. 2005; 106:3293–9. [PubMed: 15961519]
27. Burdelya LG, Krivokrysenko VI, Tallant TC, Strom E, Gleiberman AS, Gupta D, et al. An agonist of toll-like receptor 5 has radioprotective activity in mouse and primate models. Science. 2008; 320:226–30. [PubMed: 18403709]
28. Staudt LM, Dave S. The biology of human lymphoid malignancies revealed by gene expression profiling. Advances in immunology. 2005; 87:163–208. [PubMed: 16102574]
29. Green M, Michaels MG. Epstein-Barr virus infection and posttransplant lymphoproliferative disorder. American journal of transplantation : official journal of the American Society of Transplantation and the American Society of Transplant Surgeons. 2013; 13(Suppl 3):41–54. quiz.
30. Doubrovina E, Oflaz-Sozmen B, Prockop SE, Kernan NA, Abramson S, Teruya-Feldstein J, et al. Adoptive immunotherapy with unselected or EBV-specific T cells for biopsy-proven EBV+ lymphomas after allogeneic hematopoietic cell transplantation. Blood. 2012; 119:2644–56. [PubMed: 22138512]
31. Alizadeh AA, Eisen MB, Davis RE, Ma C, Lossos IS, Rosenwald A, et al. Distinct types of diffuse large B-cell lymphoma identified by gene expression profiling. Nature. 2000; 403:503–11. [PubMed: 10676951]
32. Rushlow C, Warrior R. The rel family of proteins. Bioessays. 1992; 14:89–95. [PubMed: 1533515]
33. Karin M, Lawrence T, Nizet V. Innate immunity gone awry: linking microbial infections to chronic inflammation and cancer. Cell. 2006; 124:823–35. [PubMed: 16497591]
34. Morgan MJ, Liu ZG. Crosstalk of reactive oxygen species and NF-kappaB signaling. Cell research. 2011; 21:103–15. [PubMed: 21187859]
35. Gorrini C, Harris IS, Mak TW. Modulation of oxidative stress as an anticancer strategy. Nature reviews Drug discovery. 2013; 12:931–47. [PubMed: 24287781]
36. Kardeh S, Ashkani-Esfahani S, Alizadeh AM. Paradoxical action of reactive oxygen species in creation and therapy of cancer. European journal of pharmacology. 2014
37. Lau A, Villeneuve NF, Sun Z, Wong PK, Zhang DD. Dual roles of Nrf2 in cancer. Pharmacological research : the official journal of the Italian Pharmacological Society. 2008; 58:262–70.
38. Jastroch M, Divakaruni AS, Mookerjee S, Treberg JR, Brand MD. Mitochondrial proton and electron leaks. Essays in biochemistry. 2010; 47:53–67. [PubMed: 20533900]

39. Brookes PS. Mitochondrial H(+) leak and ROS generation: an odd couple. Free radical biology & medicine. 2005; 38:12–23. [PubMed: 15589367]
40. Trachootham D, Alexandre J, Huang P. Targeting cancer cells by ROS-mediated mechanisms: a radical therapeutic approach? Nature reviews Drug discovery. 2009; 8:579–91. [PubMed: 19478820]
41. Oussaief L, Ramirez V, Hippocrate A, Arbach H, Cochet C, Proust A, et al. NF-kappaB-mediated modulation of inducible nitric oxide synthase activity controls induction of the Epstein-Barr virus productive cycle by transforming growth factor beta 1. Journal of virology. 2011; 85:6502–12. [PubMed: 21507981]
42. Lam LT, Davis RE, Pierce J, Hepperle M, Xu Y, Hottelet M, et al. Small molecule inhibitors of IkappaB kinase are selectively toxic for subgroups of diffuse large B-cell lymphoma defined by gene expression profiling. Clinical cancer research : an official journal of the American Association for Cancer Research. 2005; 11:28–40. [PubMed: 15671525]
43. Adams J. The development of proteasome inhibitors as anticancer drugs. Cancer cell. 2004; 5:417–21. [PubMed: 15144949]
44. Pan Z, Scheerens H, Li SJ, Schultz BE, Sprengeler PA, Burrill LC, et al. Discovery of selective irreversible inhibitors for Bruton's tyrosine kinase. ChemMedChem. 2007; 2:58–61. [PubMed: 17154430]
45. Honigberg LA, Smith AM, Sirisawad M, Verner E, Loury D, Chang B, et al. The Bruton tyrosine kinase inhibitor PCI-32765 blocks B-cell activation and is efficacious in models of autoimmune disease and B-cell malignancy. Proceedings of the National Academy of Sciences of the United States of America. 2010; 107:13075–80. [PubMed: 20615965]
46. Keifer JA, Guttridge DC, Ashburner BP, Baldwin AS Jr. Inhibition of NF-kappa B activity by thalidomide through suppression of IkappaB kinase activity. The Journal of biological chemistry. 2001; 276:22382–7. [PubMed: 11297551]
47. Latif T, Chauhan N, Khan R, Moran A, Usmani SZ. Thalidomide and its analogues in the treatment of Multiple Myeloma. Experimental hematology & oncology. 2012; 1:27. [PubMed: 23210501]
48. Egan LJ, Eckmann L, Greten FR, Chae S, Li ZW, Myhre GM, et al. IkappaB-kinasebeta-dependent NF-kappaB activation provides radioprotection to the intestinal epithelium. Proceedings of the National Academy of Sciences of the United States of America. 2004; 101:2452–7. [PubMed: 14983030]
49. Vodanovic-Jankovic S, Hari P, Jacobs P, Komorowski R, Drobyski WR. NF-kappaB as a target for the prevention of graft-versus-host disease: comparative efficacy of bortezomib and PS-1145. Blood. 2006; 107:827–34. [PubMed: 16174760]
50. Barth TF, Dohner H, Werner CA, Stilgenbauer S, Schlotter M, Pawlita M, et al. Characteristic pattern of chromosomal gains and losses in primary large B-cell lymphomas of the gastrointestinal tract. Blood. 1998; 91:4321–30. [PubMed: 9596681]
51. Houldsworth J, Mathew S, Rao PH, Dyomina K, Louie DC, Parsa N, et al. REL proto-oncogene is frequently amplified in extranodal diffuse large cell lymphoma. Blood. 1996; 87:25–9. [PubMed: 8547649]
52. Rao PH, Houldsworth J, Dyomina K, Parsa NZ, Cigudosa JC, Louie DC, et al. Chromosomal and gene amplification in diffuse large B-cell lymphoma. Blood. 1998; 92:234–40. [PubMed: 9639522]
53. Handy DE, Loscalzo J. Redox regulation of mitochondrial function. Antioxidants & redox signaling. 2012; 16:1323–67. [PubMed: 22146081]
54. Chen W, Balakrishnan K, Kuang Y, Han Y, Fu M, Gandhi V, et al. Reactive oxygen species (ROS) inducible DNA cross-linking agents and their effect on cancer cells and normal lymphocytes. Journal of medicinal chemistry. 2014; 57:4498–510. [PubMed: 24801734]

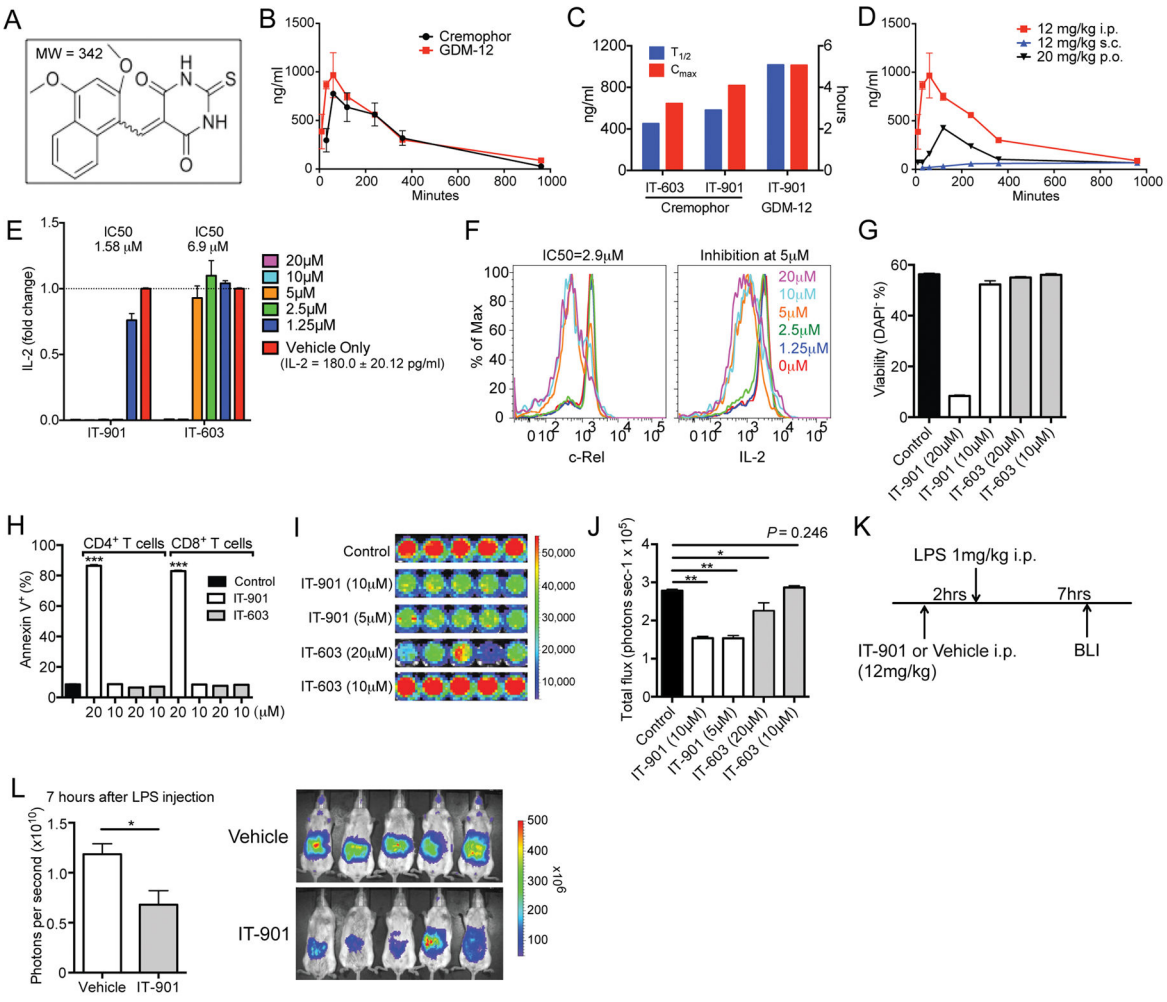

Figure 1.

IT-901 is a more potent c-Rel inhibitor than IT-603 and has a superior pharmacokinetic profile. A, Structure of IT-901. B–D, Plasma samples were analyzed at 30 minutes, 1, 2, 4, 6, and 16 hours after intraperitoneal administration of c-Rel inhibitor compounds IT-603 and IT-901. To assess the levels of IT-603 and IT-901 in blood, samples were analyzed by liquid chromatography-tandem mass spectrometry (LC-MS/MS; for more details, see Materials and Methods). B, Pharmacokinetics of IT-901 utilizing different vehicles are shown. C, Serum half-life ($T_{1/2}$) and maximum concentration (C_{max}) of IT-603 and IT-901 with different vehicles are presented. D, Pharmacokinetics of IT-901 with GDM-12 with different types of administrations are shown. i.p., intraperitoneal injection; s.c., subcutaneous injection; p.o., per oral. E and F, Wild-type C57BL/6 mouse splenocytes were treated with six different concentrations of IT-901 for one hour and analyzed after anti-CD3/CD28 stimulation for 5 hours. E, Levels of IL-2 evaluated by ELISA in the culture supernatant are shown. F, Representative flow cytometric analysis of intracellular c-Rel and IL-2 are shown. Data are representative of more than three experiments. G and H, Viability of the T cells after 24-hour incubation with different concentrations of IT-603, IT-901, or empty vehicle. Percentages of live/dead cells and Annexin-V-positive pro-apoptotic cells are shown. Values represent mean ± s.e.m. (n = 5, technical replicates). ***, $P < 0.001$ comparing IT-901 to

empty vehicle. Data are representative of more than three experiments. I and J BALB/C-Tg(NFκB-RE-luc)-Xen mice were used for *in vitro* and *in vivo* analyses of c-Rel inhibitor compounds' effects on NFκB signaling. 1×10^6 splenocytes from *NFκB-RE-luc* mice were prepared *in vitro* with 1 μg/ml of LPS on a 96-well plate. Cells were treated with different concentrations of IT-901, IT-603, or empty vehicle (control) for 24 hours and bioluminescent intensity was analyzed. I, Pseudocolor images superimposed on conventional photographs are shown. J, The bioluminescent signal intensity is shown. Data are representative of three independent experiments (I and J). Values represent mean ± s.e.m. ($n = 3$, technical replicates). *, $P < 0.05$; **, $P < 0.01$. K, *In vivo* treatment schedule of *NFκB-RE-luc* mice. L, The whole-body activation of NF-κB signal was monitored using *in vivo* bioluminescence imaging (BLI). Pseudocolor images superimposed on conventional photographs are shown. Data are representative of two independent experiments (K and L). Values represent mean ± s.e.m. ($n = 5$) *, $P < 0.05$.

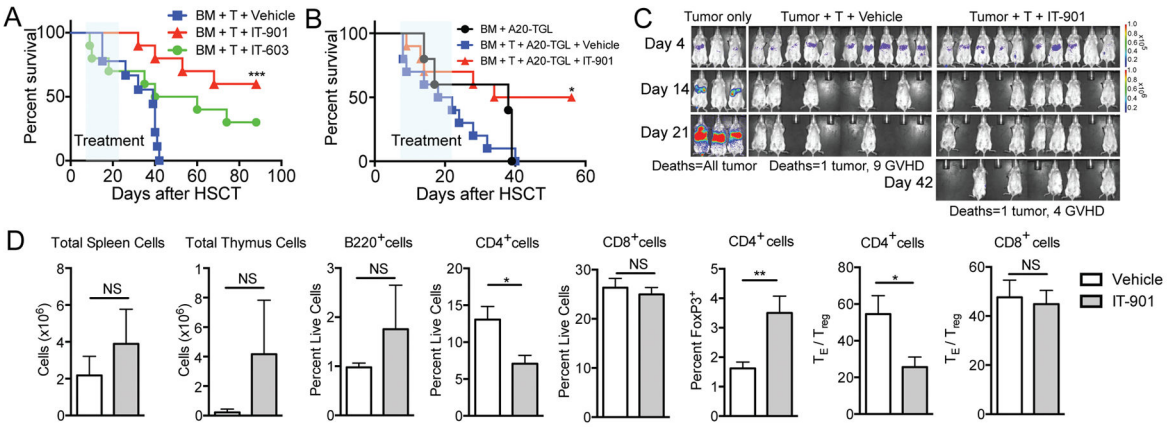

Figure 2.

c-Rel inhibitor administration is an effective treatment of acute GVHD without impairing anti-tumor activity. A, Lethally irradiated BALB/c recipients were transplanted with C57BL/6 TCD BM cells with 0.5×10^6 C57BL/6 wild-type T cells. c-Rel inhibitor compound IT-603, IT-901 or control vehicle solution was administered i.p. from day 8 (24 mg/kg, every other day for 2 weeks). Survival curve is shown. ***, $P < 0.001$ comparing recipients treated with IT-901 versus vehicle. Data are representative of two independent experiments (n = 10). B and C, Lethally irradiated BALB/c recipients were transplanted with C57BL/6 TCD BM cells with 0.5×10^6 C57BL/6 wild-type T cells. IT-901 or control vehicle solution was administered i.p. from day 8 (24 mg/kg, every other day for 2 weeks). On day 0, HSCT recipients were challenged with 0.25×10^6 luciferase-expressing A20-TGL B cell lymphoma cells. Survival curve is shown (B). *, $P < 0.05$ comparing recipients treated with IT-901 versus vehicle. Data are representative of two independent experiments (n = 3–10). The whole-body distribution of tumor cells was monitored using *in vivo* BLI. For four time points, pseudocolor images superimposed on conventional photographs are shown (C). D, Lethally irradiated BALB/c recipients were transplanted with C57BL/6 TCD BM cells with 0.5×10^6 C57BL/6 wild-type T cells. IT-901 or control vehicle solution was administered i.p. from day 8 (24 mg/kg, every other day for 2 weeks). Spleen and thymus were analyzed on day 21 after HSCT. Values represent mean ± s.e.m. ($n = 5$). Data are representative of two independent experiments. *, $P < 0.05$; **, $P < 0.01$; NS, not significant.

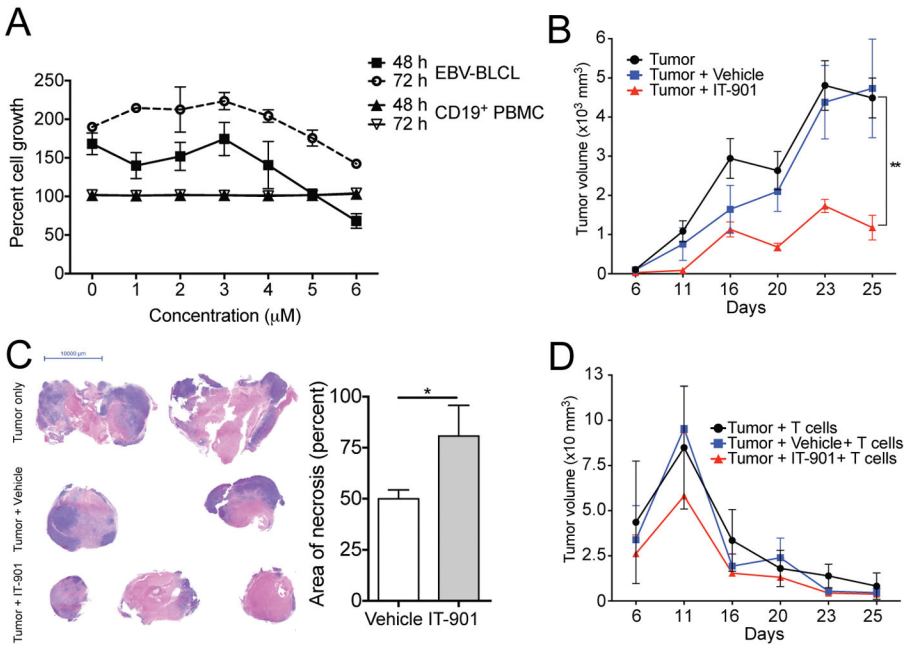

Figure 3.

IT-901 inhibits tumor growth in a xenograft model of human EBV-induced B cell lymphoma. A, Human EBV-BLCL and control human CD19^{+} PBMC were cultured for 3 days in the presence of serial dilutions of IT-901. Relative cell growth was measured by MTS Cell Proliferation Assay. Mean ± s.e.m. of technical replicates are presented. B–D, *In vivo* efficacy of IT-901 in a xenograft model of EBV-induced B cell lymphoma. B, 5×10^{6} EBV-BLCL were administered subcutaneously above the left hind leg of NSG mice. On day 8 after tumor challenge treatment with IT-901 (20 mg/kg, i.p. daily) versus vehicle or no treatment was initiated. Tumor volume was measured manually with a caliper at the indicated time points. Mean ± s.e.m. are presented (n = 5). One of two independent experiments is presented. **, P < 0.01. C, H&E staining of whole tumors harvested at day 25 after start of treatment. Left Panel; representative images of tumors harvested from the three groups. Purple areas represent viable lymphoma cells, pink areas represent necrosis. Right Panel; Area of necrosis of whole tumors was determined based on H&E staining. Mean ± s.e.m. are presented. *, P < 0.05. D, 5 × 10^{6} EBV-BLCL were administered subcutaneously above the left leg of NSG mice. All animals received three infusions of 10 × 10^{6} EBV-specific human cytotoxic T lymphocytes in weekly intervals starting day 8 after tumor challenge. In addition, treatment with IT-901 (20 mg/kg, i.p. daily) versus vehicle or no treatment was initiated on day 8 after tumor challenge. Tumor volume was measured manually with a caliper at the indicated time points. Mean ± s.e.m. are presented (n = 5). One of two independent experiments is presented.

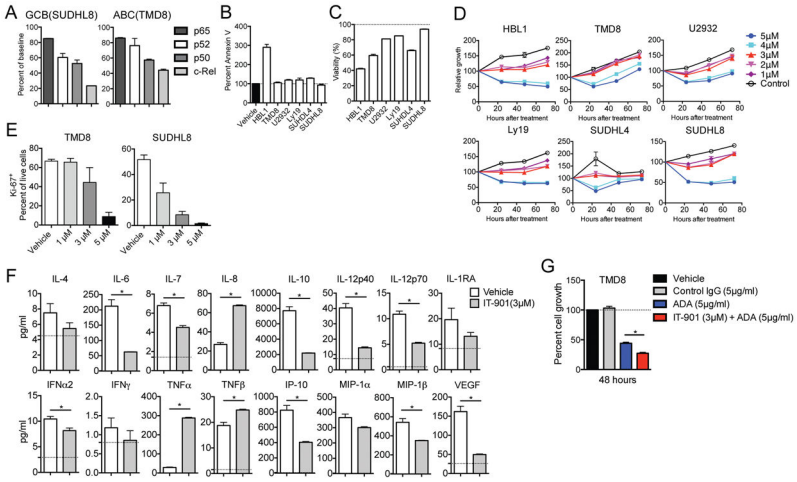

Figure 4.

IT-901 inhibits growth of human DLBCL and modulates the cytokine profile of activated B cell lymphoma cells. A, SU-DHL8 and TMD8 cells were cultured in the presence of IT-901 (3μM) or control vehicle solution for 24 hours. Nuclear translocation of four NF-κB subunits (p65, p52, p50, and c-Rel) was analyzed by flow cytometry. Values represent mean ± s.e.m. (n = 2, technical replicates). B and C, Human DLBCL cell lines were treated with IT-901 (4μM) or control vehicle for 48 hours. Annexin-V-positive proapoptotic cells are shown (B). Viability of the tumor cells after 48-hour incubation is shown in (C) (normalized values to vehicle treatment). Values represent mean ± s.e.m. (n = 4, technical replicates). Data are representative of two independent experiments. D, Human DLBCL cell lines were treated for 3 days with serial dilutions of IT-901. Relative cell growth was measured by MTS Cell Proliferation Assay. Data are representative of three independent experiments. E, TMD8 and SU-DHL8 cells were cultured in the presence of IT-901 (1~5μM) or control vehicle solution for 24 hours and viability as well as Ki-67 expression was analyzed by flow cytometry. Percentages of Ki-67$^+$ proliferating viable cells are shown. Data are representative of two independent experiments. F, TMD8 tumor cells were cultured in the presence of IT-901 (3μM) or control vehicle solution for 24 hours. Cytokine levels of the supernatant are shown (Multiplex ELISA). Mean values and s.e.m. are presented (samples were analyzed in triplicates). *, $P < 0.05$. Dotted line indicates the minimum detection limit of the assay. G, TMD8 tumor cells were cultured in the presence of IT-901 (3μM) and anti-TNF-α antibody (ADALIMUMAB; ADA) for 48 hours. Relative cell growth was measured by MTS Cell Proliferation Assay. Values represent mean ± s.e.m. (n = 4, technical replicates). *, $P < 0.05$; **, $P < 0.01$. Data are representative of two independent experiments.

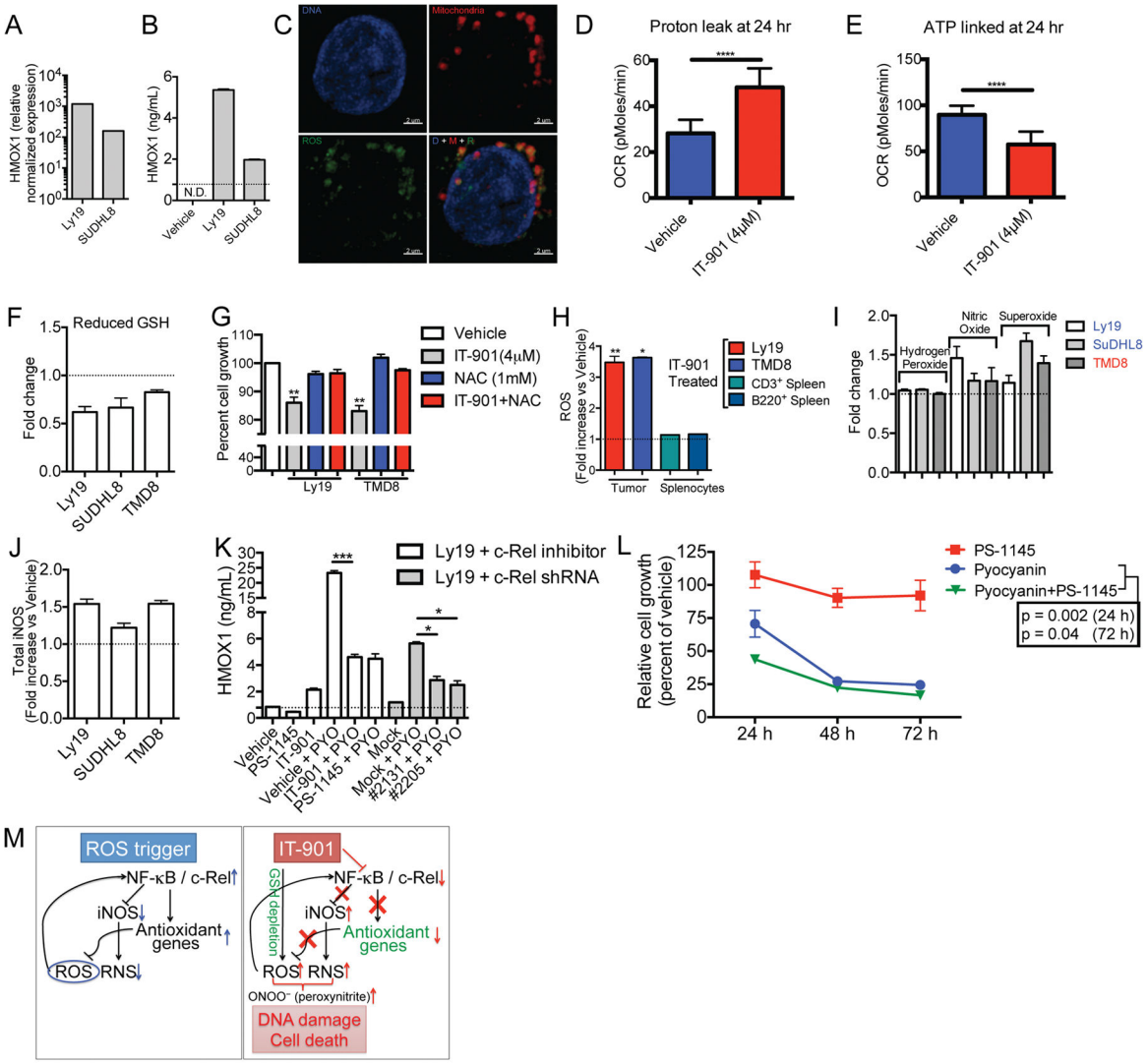

Figure 5.

Anti-lymphoma efficacy of IT-901 is mediated by oxidative stress. A and B, Ly19 and SU-DHL8 tumor cells were treated with IT-901 (4μM), or control vehicle for 24 hours. Heme oxygenase 1 (HMOX1) gene expression level by quantitative PCR and protein level by ELISA are shown (A and B), respectively. Dotted line indicates the minimum detection limit of the assay. N.D., not detected. C, SU-DHL8 tumor cells were treated with IT-901 (4μM) for 24 hours and stained with carboxy-H_2DCFDA for microscopic detection of ROS. Representative confocal microscope images are shown (blue; DNA, red; Mitochondria, green; ROS; for more experimental details, see Materials and Methods). Data are representative of two independent experiments. D and E, Ly19 cells were treated with IT-901 at 4μM or control vehicle for 24 hours and mitochondrial respiration was analyzed with extracellular flux assays (see Materials and Methods for more experimental details). Proton leak (=non-ATP linked respiration) (D) and ATP-linked oxygen consumption rate (OCR) are presented (E). ****, $P < 0.0001$. F, Ly19, SU-DHL8, and TMD8 cells were treated *in vitro* with IT-901 (4μM) or control solution for 24 hours. Cells were analyzed for

total and oxidized glutathione by HT Glutathione Assay Kit as described in Materials and Methods and the levels of reduced glutathione are presented. Values represent mean ± s.e.m. $P = 0.015$ when mean levels of reduced GSH from each cell line (n=3) were compared to control. G, Ly19 and TMD8 tumor cells were treated with IT-901 (4μM) or control vehicle solution for 24 hours with or without *N*-Acetyl-L-cysteine (NAC). Relative cell growth was measured by MTS Cell Proliferation Assay. Values represent mean ± s.e.m. ($n = 4$, technical replicates). **, $P < 0.01$. H, Ly19 and TMD8 tumor cells were treated with IT-901 (4μM) or control vehicle solution for 24 hours to analyze reactive oxygen species (ROS). Wild-type C57BL/6 mouse splenocytes were also cultured in the same condition. ROS levels were analyzed by utilizing a fluorogenic marker (carboxy-H_2DCFDA) and normalized to the level of vehicle treated cells. Values represent mean ± s.e.m. ($n = 4$, technical replicates). *, $P < 0.05$; **, $P < 0.01$. I, Ly19, SU-DHL8, and TMD8 tumor cells were treated with IT-901 (4μM), or control vehicle for 24 hours. Levels of hydrogen peroxide, nitric oxide, and superoxide after the treatment are shown (normalized values to vehicle treatment, dotted line indicates the level of control vehicle treated group). Values represent mean ± s.e.m. ($n = 3$, technical replicates). Data are representative of two independent experiments. J, Ly19, SU-DHL8, and TMD8 cells were treated *in vitro* with IT-901 (4μM) or control solution for 24 hours. Total iNOS levels are shown in as determined by cell-based human total iNOS immunoassay kit (ELISA). $P = 0.023$ when mean iNOS activities from each cell line (n=3) were compared to control. K, Ly19 tumor cells were treated with pyocyanin (PYO) to generate high levels of oxidative stress in the presence of vehicle versus IT-901 or PS-1145 (at 4μM, open bars), or in the presence of mock versus c-Rel-specific shRNA (#2131 and #2205, gray bars) for 24 hours, followed by analysis of HMOX1 induction. HMOX1 protein level by ELISA is shown. Dotted line indicates the minimum detection limit of the assay. Values represent mean ± s.e.m. ($n = 5$, technical replicates). *, $P < 0.05$; ***, $P < 0.001$. See Materials and Methods for more experimental details. L, Ly19 cells were treated for 3 days with PS-1145 (4 μM), pyocyanin (350 μM), or PS-1145 (4 μM) + pyocyanin (350 μM). Relative cell growth was measured by MTS assay. Combined data from two independent experiments are presented. M, The proposed effects of IT-901 on oxidative stress induction and the oxidative stress response in lymphoma cells. Left panel: upon ROS induction, HMOX1 is upregulated through NF-κB activation and this serves as an antioxidant response. At the same time, the level of iNOS is expected to be decreased as iNOS production is negatively regulated by the NF-κB pathway. Impacts of ROS induction are indicated by blue arrows. Right panel: in the setting of IT-901 treatment, three major responses are observed; 1. Buildup of ROS as a result of GSH depletion, 2. Suppression of HMOX1 due to decreased NF-κB/c-Rel activity, which weakens the oxidative stress response, 3. Induction of iNOS by inhibiting its negative regulator NF-κB/c-Rel, resulting in production of nitric oxide. Increased production of ROS/RNS contributes to the production of peroxynitrite, which exacerbates ROS-mediated DNA damage and cell death. Impacts of IT-901 are indicated by red arrows and cross marks. Changes that affect ROS removal are shown in green.